Interaction of Langmuir wave packets with streaming electrons: Phase-correlation aspects

L. Muschietti, I. Roth, and R. Ergun
Space Sciences Laboratory, University of California, Berkeley, California 94720

(Received 29 November 1993; accepted 3 January 1994)

An analytical model of the interaction between a localized wave packet and energetic electrons is presented. Electrostatic packets of tens to a hundred wavelengths are considered in order to emulate the Langmuir waves observed in the auroral zone and in the solar wind. The phase information is retained, so the results can be applied to wave–particle correlator measurements. The perturbed distribution function is explicitly calculated and is shown to be bounded over all phase space due to a broadening of resonance ascribable to the finite extent of the packet. Its resistive part (in phase or 180° out of phase with the electric field) maximizes for $v=\omega/k$, so that the associated bunching of electrons enables assessment of the characteristic wavelength. The changes in the wave profile due to the interaction with the energetic electrons are calculated. Broad wave packets grow or decay "self-similarly" with a rate given by the standard expression for a plane wave. Narrow, growing packets, on the other hand, quickly widen to sizes determined by the local distribution function. This sets a lower bound to the sizes of observed packets. Present results are supported by test-particle simulations and are in accord with recent correlator data of intense, localized Langmuir waves in the auroral zone.

I. INTRODUCTION

Many phenomena in plasma physics involve the microscopic interaction between wave fields and particles in phase space, and thus require a kinetic description. Yet the application of kinetic theory to space plasmas is fraught with difficulties in the interpretation of experimental data. One main difficulty stems from the relative motion between the plasma and the satellite or rocket probing it. The interpretation of microinstabilities, such as the classic example of high-frequency Langmuir waves excited by a bump on tail, requires measuring both wave fields and electron distribution functions at the same location. In cases where the waves have been measured simultaneously with particle distributions, only estimates of the growth rate could be obtained.

In the solar wind, measurements of electron distributions by satellite take $\sim$10–60 s,[1] which means, accounting for the solar wind speed, that a large span (4000–24 000 km) of plasma is covered. On the other hand, Langmuir emissions have been reported since the early observations[2] by the Helios satellite to be highly inhomogeneous and intermittent. They are sometimes described as clumpy.[3] Intensity variations over two orders of magnitude can occur within 0.5 s and the most intense bursts reach $\sim$1 mV/m, more than three orders of magnitude above the background electric field. Though the packets of Langmuir waves show considerable variability, their spatial dimensions[4] can be assessed as 20–100 km. In view of the large discrepancy between the latter scale and the region covered by one measurement of the electron distribution, it is hard to establish a direct quantitative link between wave fields and distributions.

Nevertheless, Lin *et al.*[1,5] were able to show that the Langmuir waves were associated with the presence of a positive slope in the electron distribution function that was reduced along the local magnetic field. The source for the streaming energetic electrons (2–10 keV) is a solar flare from which they escape into the interplanetary space. Velocity dispersion, whereby faster electrons run ahead of the slower ones, forms a time-dependent positive slope in the distribution function and leads to a spectrum of Langmuir waves slowly shifting from high to low phase velocities.[6–8] The growth rate of $\gamma \lesssim 1\ s^{-1}$ inferred from the measured slope[1,5] was shown, however, to be too small to allow the waves to grow at all for conditions prevailing in the solar wind.[9] It is now believed that much larger slopes and, hence, growth rates are locally present, whose actual values are masked in the particle measurements by an averaging over several thousand km.[10,11] Thus, even as basic a question as what is the growth or decay rate of the Langmuir waves in the solar wind remains experimentally unanswered. Typical data regarding observations of Langmuir waves in the solar wind are summarized in Table I.

Langmuir waves have also been observed in the auroral zone by rockets launched to altitudes of <1000 km.[12] Here also the emissions appear clumpy and intermittent. The electrostatic field amplitude can vary from a few mV/m to 100 mV/m in 0.2 s. Intense Langmuir waves with amplitudes over 200 mV/m appear in bursts of $\sim$0.1 s duration.[13] The waves are observed in association with fluxes of precipitating electrons in the 0.3–3 keV range, which are generated and strongly modulated at altitudes of $\sim$6000 km.[14] Velocity dispersion of these electrons, as they propagate toward lower altitudes, results in a time-dependent positive slope in the local distribution functions, similar to the scenario for the solar wind. Present sounding rockets are equipped with recently developed particle instruments, which have faster time resolution than those on board satellites flown in the solar wind, and the measure-

 1070-664X/94/1(4)/1008/17/$6.00

TABLE I. Observational parameters.

Description	Symbol	Solar wind	Aurora
Plasma frequency	ω_p	$1\text{–}2\times10^5$ s^{-1}	9×10^6 s^{-1}
Electron thermal velocity	v_e	1.5×10^6 m s^{-1}	2×10^5 m s^{-1}
Beam velocity	v_b	$3\text{–}5\times10^7$ m s^{-1}	$1\text{–}3\times10^7$ m s^{-1}
Range of velocities with positive slope	$\Delta v_+/v_b$	0.1–0.2	0.1–0.2
Resonant wave number	k_b	$1\text{–}3\times10^{-3}$ m^{-1}	0.5 m^{-1}
Estimated size of a packet	$2L$	$2\text{–}10\times10^4$ m	$1\text{–}10\times10^2$ m
Electric field amplitude:	$2E_0$		
typical		3×10^{-5} V m^{-1}	$1\text{–}10\times10^{-2}$ V m^{-1}
maximum		$1\text{–}2\times10^{-3}$ V m^{-1}	0.5 V m^{-1}
Estimated growth rate	γ	$\geqslant10$ s^{-1}	300 s^{-1}
Transit time of a resonant electron	τ_t	$0.2\text{–}3\times10^{-4}$ s	$0.3\text{–}1\times10^{-5}$ s

ments of electron distributions take >256 ms. This time is still too long to resolve a 100 m packet of Langmuir waves that passes by in 0.1 s. Nevertheless, a coarse parallel distribution can be obtained in ~4 ms. These observations show positive slopes in parallel velocities (not integrated over $v_\perp$), and the signature of the dispersion in energetic electrons. One cannot, however, assess the wave growth rate accurately nor derive information on the kinetic interaction between the waves and the electrons.

In order to circumvent the difficulties just described, wave–electron correlators are now being developed.[15,16] These instruments can follow the actual phase of the high-frequency Langmuir fields and search for a possible correlation between that phase and the arrival times of energetic electrons in the particle detector. The technique has already enabled direct identification of the resonant electrons in the auroral zone, and thus assessment of the typical wavelength.[13] Data analysis shows that the waves are spatially localized in packets with dimensions of tens to a hundred wavelengths, packets that therefore ought to be distinguished from the envelopes with a vanishing wave number discussed in strong turbulence theory.[17] Data pertaining to Langmuir waves in the auroral zone are also summarized in Table I.

From a theoretical viewpoint, a model of wave–particle interaction that applies to the aurora or to the solar wind should account for the following: (1) the region of the wave packet is traversed by a flux of "resonant" electrons that have only a finite transit time τ_t to interact with the packet; and (2) the wave field is coherent over time scales larger than τ_t. The assumption of coherence is, of course, at the core of a wave–particle correlator, which by definition operates at a level where the phase of the field is nonrandom. By contrast, weak turbulence theory does not incorporate the wave phase, just its modulus. Standard trapping theory assumes an infinite wave train without spatial localization. The goal of our research is to provide an analytical model that pinpoints the peculiarities of the wave–particle interaction due to the finite size of the wave packet, and helps the interpretation of the correlator data. This program can be achieved by combining Vlasov and Poisson equations in a model, where the coherent field is explicitly limited to a packet, in a way suggested by Denavit and Sudan.[18] Because for our applications Langmuir waves have a phase velocity well distinct from the dense background of electrons, dispersion relation and evolution of the packet envelope can be decoupled. Moreover, because the transit time τ_t is shorter than the trapping period, the Vlasov equation can be linearized, and is analytically integrated.

For a packet with an amplitude $2E_0$ and extension $2L$, the two main parameters controlling the features of the interaction are $\sigma\equiv(kv-\omega)\ (L/v)$ and $\mu\equiv(2eE_0k/m\omega^2)\ (kL)^2$. The first one, which represents the Doppler-shifted frequency seen by the traversing electrons times the duration of their transit through the packet, is important to distinguish between resonant and nonresonant particles. It couples wave properties with particle velocities and spatial profile of the packet. The second one, which is a measure of the effect of the localized electric field on the electrons, is used as an expansion parameter to compute iteratively perturbations in the distribution function. It can be thought of as the transit duration τ_t times the trapping frequency, and clearly the validity of the perturbation analysis is limited to localized fields. For a Gaussian packet, explicit analytical expressions are obtained for the linear perturbed distribution function. The perturbation does not become singular for resonant electrons because these have a short; finite transit time to exchange energy with the localized packet. For the same reason there is a broadening of the resonance at $v_p=\omega/k$, whose width is determined by $(kL)^{-1}$ (see Fig. 1 to assess the significance of the effect). The phase bunching of resonant electrons is predicted to be in phase with the electric field, which is consistent with the observations.[19] When the packet dimension is sufficiently large, the energy exchanged with the perturbed electrons agrees with the classical expression, namely the packet amplitude grows or decays exponentially with a rate proportional to the slope of the velocity distribution function evaluated at the phase velocity v_p. If resonant electrons are significantly perturbed by the wave field, i.e., $\mu>0.2$, the nonlinear effects must be taken into account.[18,20] As will be shown in a subsequent publication, they may lead to an enhanced localization of the wave field.[21]

Since the pioneering work of Landau,[22] many studies have addressed the spatial development of a high-frequency electrostatic field interacting with plasma electrons. Several coherent aspects of the interaction were investigated over 20 years ago, in connection with laboratory plasma experiments. Spatial echos were predicted by the theory[23] and observed in a large plasma column,[24] confirming the existence of streaming oscillations in the distribution function.[22] The nonlinear amplitude oscillation of a large-amplitude electron plasma wave caused by the bouncing motion of trapped electrons,[25] was observed by Malmberg and Wharton.[26] Their experiment dealt with the spatial damping and oscillation of the large-amplitude wave. After a few bounces the energy exchange between wave and resonant electrons ceases, and the wave settles to a constant level.[27] The associated observation of growing sideband waves led to a great deal of theoretical work on the stability of a large-amplitude wave that is supported by a distribution of trapped electrons localized near the bottom of the potential troughs.[28] Later, Morales and Malmberg[29] unveiled a link between the question of sideband generation and the echo phenomenon. Linear sidebands arise from the coupling of the launched wave to low-frequency streaming perturbations in the electron distribution function; as a result, their amplitude exhibits large spatial oscillations, while the launched wave damps monotonically. The interaction between Langmuir wave and streaming perturbations was investigated further both theoretically and experimentally by Gervais *et al.*[30]

Other studies, not based on the Vlasov equation, consider the interaction between sharply localized oscillating electric fields and electrons. They are set up to either determine the strength of the damping on the field due to transit time effects[31] or to characterize the statistical effects on the electron distribution function resulting from its encounter with many localized fields.[32,33] The statistical approach assumes that each clump involves a relatively small electric field that imparts an average "kick" in the velocity (energy) of the electron. The effect of multiple packets having different shapes and amplitudes on the electrons is calculated in an average sense via a diffusion operator. In the solar wind applications, Melrose and Cramer[33] showed that the inhomogeneous clumps can be incorporated in the quasilinear diffusion operator, thus justifying the success of Grognard's calculations,[34] which balance the effects of velocity dispersion by quasilinear diffusion on the distribution function. The effects of a single, intense, solitary-like structure on passing electrons were investigated, mainly in the context of strong turbulence, because transit-time effects are considered crucial for the arrest of Langmuir wave collapse.[35] The wave energy is extracted by bulk electrons resulting in the formation of tails in the distribution function.[32,36,37] Several laboratory experiments[38] investigated the effects of a super-strong Langmuir turbulence (with normalized wave energy $W/nT_e > 1$), and its interaction with an electron beam. In sharp contrast to those strong turbulence studies we consider in this paper much weaker electric fields and much less localized structures. From Table I we find for the peak values, $W/nT_e < 10^{-3}$ in the auroral zone and $W/nT_e < 10^{-5}$ in the solar wind. Furthermore, the typical dimensions of the packets we discuss read in units of Debye length $2L/\lambda_d \sim kL(v_p/v_e) = 10^3$–$10^4$, i.e., two orders of magnitude larger than the $\sim 20\ \lambda_d$ structures envisioned in the strong turbulence transit-time studies. For those two reasons, ponderomotive effects are discarded in the present study. Rather, we focus on the phase bunching of the interacting electrons and, simultaneously, on the evolution of the Langmuir packet due to the lowest-order energy exchange with the particles.

TABLE II. Selected theoretical parameters.

Description	Symbol	Value
Phase velocity	v_p/v_e	20–100
Growth rate	γ/ω_p	$>10^{-4}$
Packet scale size	kL	10–100
Transit time	$\omega_p\tau_t = kL$	10–100
Normalized field	$\mu = \frac{2E_0ek}{m\omega_p^2}(kL)^2$	0.01–0.2

In Sec. II we present the general expressions of distribution functions perturbed by a localized field and their in- and out-of-phase relations with the field. We also introduce equations to describe how the field itself is affected by the interaction. In Sec. III we explicitly calculate the perturbation for the streaming electrons. We obtain the correction of the distribution as a function of position and velocity, point out the important modifications due to the finite size of the packet, and compare the results to those of test-particle simulations. In Sec. IV we deal with the evolution of a wave packet due to the interaction with the traversing electrons. The energy exchanged is calculated explicitly from the perturbed distribution and compared to data from test-particle simulations. In Sec. V we summarize our results and discuss their applications to present and future experiments in space.

II. FINITE-SIZE WAVE PACKET IN A VLASOV PLASMA

We consider a coherent, localized packet propagating in the x direction with a phase $\psi(x,t)$. The coherence time is assumed longer than the transit time τ_t of electrons through the packet, which requires it to be longer than 10–100 plasma periods (see Table II). The localization of the electrostatic field is specified by a form factor $\eta(x,t)$ piecewise continuous, bounded, and vanishing for $x \to \pm\infty$. Its slow time dependence describes the drift due to the group velocity of the Langmuir waves or the growth (or damping) due to the interaction with the electrons. Explicitly, the field is written as

$$E(x,t) = E_0\eta(x,t)\exp(i\psi) + \text{c.c.}, \tag{1}$$

where c.c. denotes the complex conjugate. The frequency, wave number, and phase velocity are given by $\omega = -\partial\psi/\partial t$ (assumed to be constant since the medium is time stationary), by $k = \partial\psi/\partial x$, and by $v_p = \omega/k$, respectively.

The electron distribution function consists of two populations: a dense background $F_0(v)$ and energetic, streaming electrons $F_e(v)$, which include velocities around v_p. The streaming density $n_e=\int dv\, F_e$ is several orders of magnitude smaller than the background density n_0. Under the influence of the wave field, both populations ($\alpha=0,e$) develop a time-dependent, inhomogeneous component $f_\alpha(x,v,t)$, which satisfies the Vlasov equation

$$\frac{d}{dt}f_\alpha\equiv\left(\frac{\partial}{\partial t}+v\frac{\partial}{\partial x}\right)f_\alpha=\frac{eE}{m}\frac{\partial}{\partial v}(F_\alpha+f_\alpha). \tag{2}$$

Poisson's equation, in turn, links the two perturbed densities with the electrostatic field of Eq. (1). Our goal is to find explicit expressions for $f_0(x,v,t)$ and $f_e(x,v,t)$ in order to analyze their phases versus the wave phase ψ for correlator applications. Neglecting the perturbation f_α on the right-hand side of Eq. (2) gives the linear approximation to the perturbed distribution function,

$$f_\alpha^{(l)}(x,v,t)=\frac{eE_0}{m}\int_{-\infty}^{t}dt'\,\eta(x',t')e^{i\psi(x',t')}\frac{\partial}{\partial v'}F_\alpha(v')+\text{c.c.}, \tag{3}$$

where the integration is carried out along the trajectories $x'(t')$, $v'(t')$, which satisfy $x'(t)=x$ and $v'(t)=v$, and we ignore the perturbation at large negative times when $x'\to\pm\infty$. The linear perturbation $f_\alpha=f_\alpha^{(l)}$ oscillates in time like the electric field, i.e., with frequency ω. From Eq. (3), one observes that the standard solution for a plane wave with a homogeneous amplitude ($\eta=1$) can be significantly modified due to the finite extension of the form factor η. The perturbed distribution function f_α depends on the structure of the form factor along the past trajectories of the particles, which constitute the unperturbed distribution function. The form factor modifies, in particular, the phase shift between the perturbed distribution function and the wave field.

Equation (3) for the background distribution f_0 is integrated as follows.[18] The variable of integration is changed from t' to $\psi[x'(t'),t']$, which is legitimate for the background electrons, since $d\psi=(kv'-\omega)dt'$ has a constant sign. Then, integrations by parts are performed to create a series in powers of $k^{-1}\partial\ln\eta/\partial x$, ratio of the fast variation scale in ψ to the slow scale in η. The first two terms of the expansion yield

$$f_0(x,v,t)=2A_0\frac{\partial F_0}{\partial v}\left\{\frac{\eta}{kv-\omega}\sin\psi+\left[v\left(\frac{\partial\eta}{\partial x}\right)+\frac{\partial\eta}{\partial t}\Big/(kv-\omega)^2-v^2\eta\left(\frac{\partial k}{\partial x}\right)\Big/(kv-\omega)^3\right]\cos\psi\right\}, \tag{4}$$

where $A_0\equiv eE_0/m$. At the lowest order (the first term on the right-hand side), the perturbation is $\pi/2$ out of phase with the electric field, which reproduces the standard result for an infinite wave train. The packet inhomogeneity, however, introduces a component in phase with the electric field. The density n_0 consists of similar components, and it will be shown in Sec. IV that the perturbed density of energetic electrons can also be split into a resistive and a reactive component: $n_e(x,t)=n_c\cos\psi+n_s\sin\psi$, where n_c, n_s are proportional to the first and second derivatives of F_e at v_p, respectively. Therefore, the sin ψ (reactive) component of Poisson's equation results in

$$2A_0\eta(k-\omega_p^2I)=\omega_p^2n_s, \tag{5a}$$

while the cos ψ (resistive) component gives

$$2A_0\frac{\partial\eta}{\partial x}+2A_0\omega_p^2\left(\frac{\partial\eta}{\partial t}\frac{\partial I}{\partial\omega}-\frac{\partial\eta}{\partial x}\frac{\partial I}{\partial k}-\frac{\eta}{2}\frac{\partial k}{\partial x}\frac{\partial^2 I}{\partial k^2}\right)=-\omega_p^2n_c, \tag{5b}$$

where the velocity integral $I=\int dv(\partial F_0/\partial v)\,(kv-\omega)^{-1}$ is introduced.[18] The latter is related to the real part of the dielectric function, as determined by the dense background,

$$\epsilon(k,\omega)=1-(\omega_p^2/k)I. \tag{6}$$

Equation (5a) yields the dispersion relation and indicates that frequency and wave numbers are related by the standard dispersion relation if the perturbed density of the streaming electrons does not contain a reactive component, $n_s=0$. It will be shown below that n_s is indeed negligible, provided that $v\partial\ln|\partial F/\partial v|/\partial v\ll kL$ and as long as $\mu\ll 1$. Therefore, k is assumed to be constant and, introducing the group velocity,

$$u\equiv\frac{d\omega}{dk}=1-\omega_p^2\frac{\partial I}{\partial k}\Big/\omega_p^2\frac{\partial I}{\partial\omega}, \tag{7}$$

Eq. (5b) simplifies to

$$2A_0\left(\frac{\partial\eta}{\partial t}+u\frac{\partial\eta}{\partial x}\right)=\frac{\omega_p^2}{k}\left(\frac{\partial\epsilon}{\partial\omega}\right)^{-1}n_c. \tag{8}$$

The wave packet propagates at the group velocity, while its amplitude is modified by the resistive component n_c of the perturbed streaming electrons. That equation will be used in Sec. IV to calculate the growth or damping of the packet.

III. DISTRIBUTION FUNCTION OF STREAMING ELECTRONS

The energetic part of the perturbed distribution function f_e affects only slightly the dispersion relation, Eq. (5a), and the wave evolution, Eq. (8); therefore, in the calculation of f_e itself we approximate the spatial derivative of the phase ψ by a constant k, giving $\psi=kx-\omega t$. Taking as characteristics the trajectories $v'(t')=v$, $x'(t')=x+v(t'-t)$, where v is assumed to be positive, Eq. (3) becomes

$$f_e(x,v,t)=A_0\,e^{i(kx-\omega t)}\frac{\partial F_e}{\partial v}\int_{-\infty}^{0}d\tau\,\eta(x+v\tau,\tau+t)e^{i(kv-\omega)\tau}+\text{c.c.}, \tag{9}$$

in which the integral over τ describes the relative phase of the oscillating perturbed distribution f_e versus the wave

phase. Equation (9) is similar in form to the one used by Landau;[22] however, our boundary conditions differ, in that non-negligible wave amplitude is limited to a finite spatial domain while the plasma medium is infinite.

The integral in Eq. (9) relates the distribution f_e to the motion of the particles at earlier times, and the effect of spatial gradients in the electric field amplitude will be directly seen in the resulting phase relation. Considering the simple stationary profile of a square window,

$$\eta(x)=\begin{cases}0, & x<0,\ x>L,\\ 1, & 0<x<L,\end{cases}$$

which has two one-point discontinuities in the electric field, one obtains, directly from (9),

$$f_e(x,v,t)=A_0\frac{i}{\omega-kv}e^{i\psi}\frac{\partial F_e}{\partial v}\left[\frac{1-e^{i(\omega/v-k)x}}{\beta-e^{i(\omega/v-k)x}}\right]+\text{c.c.}\quad\begin{matrix}0<x<L,\\ L<x,\end{matrix}\tag{10}$$

where $\beta=\exp[i(k-\omega/v)(L-x)]$. Converting space to time, the solution for $0<x<L$ is equivalent to Eq. (6) of O'Neil.[25] In the square bracket, the rightmost exponents reflect the presence of the left boundary, while β reflects the right boundary in the wave field. They modify the phase of the perturbation relative to the wave phase ψ and yield also, downstream of the interaction region, a ballistic term $\exp[i(k-\omega/v)x]$, which carries information on the number of oscillations felt by the particles during their transit. Another point to note is that the presence of these boundary terms plays an essential role in keeping bounded the perturbed distribution function of resonant electrons. The usual expression for a plane wave [Eq. (10), with the square bracket equal to unity] shows the perturbation to have a singularity at resonance; therefore, the assumed linear solution breaks down. Instead, the expression above can be expanded for velocities close to v_p and, following O'Neil, secular terms sought after. As a result, the derivative that was neglected in the linearization of (2) is evaluated at the phase velocity as

$$\left.\frac{\partial f_e}{\partial v}\right|_{v_p}\sim\left\{-2\cos\psi\left[v_p^{-1}-\partial\left(\ln\left|\frac{\partial F_e}{\partial v}\right|\right)\Big/\partial v\right]kx+\sin\psi\, v_p^{-1}(kx)^2\right\},$$

so is dominated by a term that grows quadratically with the distance. Thus, to guarantee the validity of the linear solution, we set a bound to $\partial f_e/\partial v$ at $x=L$ by requiring

$$\frac{eE_0k}{m}\left(\frac{kL}{\omega}\right)^2<1,\tag{11}$$

i.e., the interaction time between the wave and the resonant particles passing by is shorter than the trapping period. This condition, albeit obtained with a simplified form factor, gives the correct expansion parameter for the validity of a linearized solution for a more realistic wave packet.

In the auroral region, as well as in the solar wind, the observed electron beams appear as little bumps at a velocity v_b riding on a nonthermal tail of the electron distribution function. In this description the range of velocities for which the reduced distribution function shows a positive slope at a given time is somewhat narrow: $\Delta v_+/v_b\sim 0.1$. The associated narrow range of wave numbers excited, $\Delta k/k\sim 0.1$, corresponds to a wave packet of width $\Delta k^{-1}\sim 10k^{-1}$. Since the dispersion of Langmuir waves is quadratic, a Gaussian envelope moving at the group velocity describes well a propagating Langmuir packet (e.g. Ref. 39). The packet disperses on a characteristic time scale $\tau_d\sim(kL)^2(v_p/v_e)^2\omega_p^{-1}$, where v_e is the electron thermal velocity. The dispersion time is for our applications very large (Table II), being several orders of magnitude larger than the transit time of resonant electrons through the packet: $\tau_d\sim 10^4\tau_t$. For simplicity, we choose to describe the wave field by a moving Gaussian packet with a fixed half-width L and group velocity u,

$$\eta(x,t)=e^{-(x-ut)^2/4L^2}.\tag{12}$$

This choice will enable us to use known properties of the complex error function to carry out the analysis and to write down explicit expressions. Substitution of Eq. (12) into (9) results in

$$f_e(x,v,t)=A_0\eta(x,t)e^{i(kx-\omega t)}\frac{\partial F_e}{\partial v}\frac{L}{v-u}\frac{1}{i}Z(\xi)+\text{c.c.},\tag{13}$$

where $Z(\xi)=2ie^{-\xi^2}\int_{-\infty}^{i\xi}e^{-s^2}\,ds$ is the plasma dispersion function with the complex argument $\xi\equiv(\omega-kv)L/(v-u)-i(x-ut)/(2L)$. The real argument of the Z function is the Doppler-shifted frequency experienced by a passing electron times its transit duration through the wave packet. The imaginary argument represents the electron position with respect to the center of the packet. Both parameters are of major importance, hence we define

$$\sigma\equiv-\mathrm{Re}(\xi)=(kv-\omega)L/(v-u),\tag{14a}$$

$$\chi\equiv-\mathrm{Im}(\xi)=(x-ut)/(2L).\tag{14b}$$

The parameter σ determines the proximity to resonance during the interaction with the localized wave packet. Exactly at resonance, $\sigma=0$. On the other hand, electrons with $|\sigma|>2$ may be considered as nonresonant. Since in all applications $u/v_p<0.01$, we set u to zero from now on for the sake of simplicity. As shown by Eqs. (14), it is always possible to include the effect of the group velocity by changing coordinates to a frame moving with u.

The class of resonant electrons depends closely upon the size of the packet. When the dimension of the packet increases, $L\to\infty$ while x remains finite, we have $\xi\to\xi_r\to\infty$ and $Z\to-1/\xi_r$. Therefore, from Eq. (13) we recover the standard result for the perturbation by a plane wave,

$$f_e(x,v,t)=iA_0\frac{\partial F_e/\partial v}{\omega-kv}e^{i(kx-\omega t)}+\text{c.c.}$$

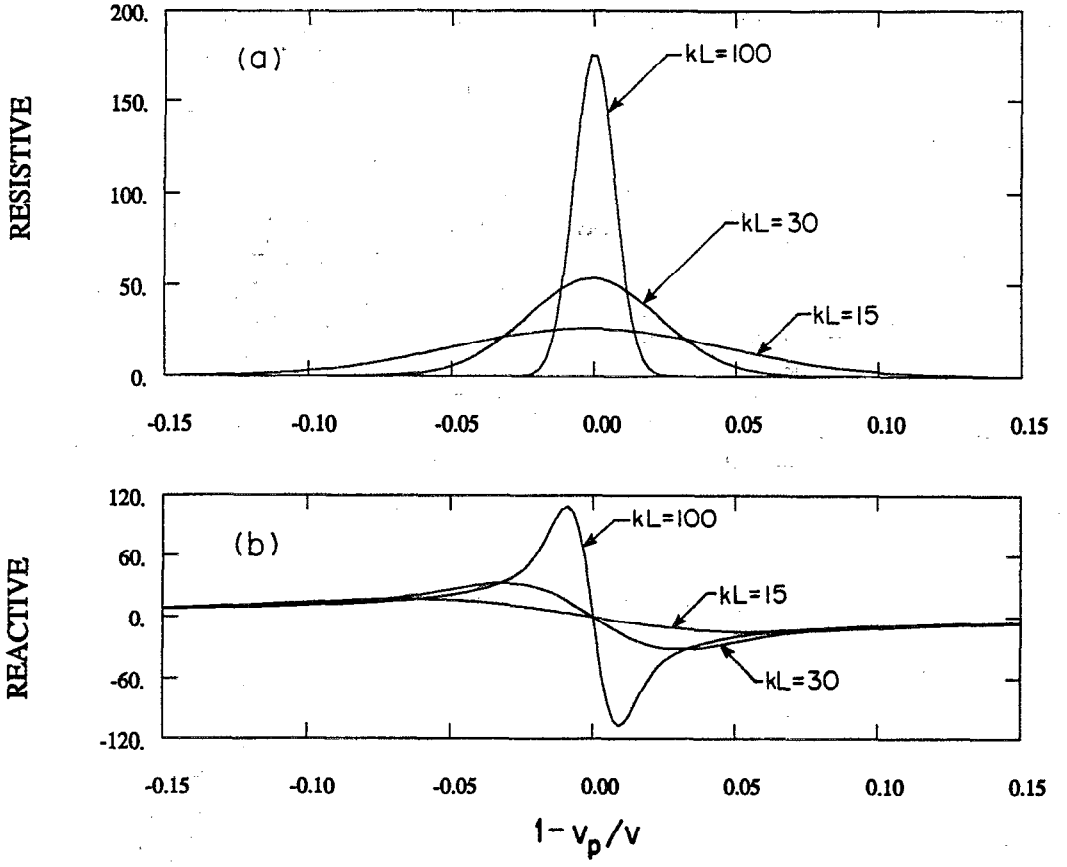

FIG. 1. Components of the resonance function defined by Eq. (15); $\sigma=(kv-\omega)L/v$. (a) Real and (b) imaginary parts are shown as a function of $(1-v_p/v)$ for three sizes of packets. The resistive component is described by a Gaussian and the reactive component by a Dawson integral. For extended packets ($kL\to\infty$), they tend to $\pi\delta(kv-\omega)$ and principal part $P[1/(kv-\omega)]$, respectively. Note the broadening of the resonance for compact packets.

By comparing that expression to Eq. (13) (with $u=0$) evaluated at the center of the packet, $x=0$, we can find a resonance function,

$$R=\frac{-iL}{v}Z(-\sigma)=\frac{-iL}{v}\left(i\sqrt{\pi}e^{-\sigma^2}+2e^{-\sigma^2}\int_0^{\sigma}e^{t^2}\,dt\right). \tag{15}$$

The real part of R, which physically represents the resistive contribution, is mathematically associated to the Gaussian $e^{-\sigma^2}$, or

$$\mathrm{Re}(R)=\pi\frac{1}{\sqrt{\pi}}\frac{L}{v}\exp\left(-\frac{L^2}{v^2}(kv-\omega)^2\right). \tag{16}$$

When $\omega L/v\to\infty$, namely the transit time becomes large, $\mathrm{Re}(R)$ tends to the usual delta function from the Plemlj formula, $\pi\delta(kv-\omega)$. It may also be shown that the imaginary part of R, associated to a Dawson integral, reduces to the principal part of $1/(kv-\omega)$. Plots of real and imaginary parts of R are shown in Fig. 1 for various sizes of packets. Height and width of the resonance are given by kL and $1/kL$, respectively. In panel (a), one clearly sees the tendency to a delta function for large values of kL and the broadening of the resonance caused by the localization of the packet. For the sake of clarity, we should stress that this broadening is a physical process distinct from the standard resonance broadening discussed in plasma physics theory.[40] To be sure, in both cases the broadening in the frequency domain reflects a limitation of the interaction time. However, in the latter case, it is the randomization of the particle orbits in a turbulent field that causes a loss of the phase relation between wave and resonant particle after a finite time interval. Because this time interval is inversely proportional to the square of the electric field, the process is nonlinear and distinct from the simple, linear broadening described in this paper.

Equation (13) gives the general linear expression for the perturbed distribution in the presence of a localized Gaussian packet. Its form shows that the perturbation follows the wave, but has an additional phase that is described by the Z function. Although we could have expressed (13) by means of a complex error function, we prefer, however, to cast f_e in the form (13) because of the common knowledge of the plasma dispersion function. We recall, for example, the familiar asymmetry of Z when its complex argument crosses the real axis. Since here the imaginary part of the argument depends on position, we expect an asymmetry of $f_e(x,v,t)$ with respect to x. Physically, this reflects the fact that we choose electrons with $v>0$, hence electrons at $x<-L$ have been hardly subjected to the interaction with the field, while electrons at $x\gtrsim L$ have felt most of its effect. If those are exactly at resonance, then

$\mathrm{Re}(\xi)=0$ and Z can be expressed by means of the error function to yield

$$f_e\left(x,\frac{\omega}{k},t\right)=2A_0\cos(kx-\omega t)\times\frac{kL}{\omega}\frac{\partial F_e}{\partial v}\bigg|_{\omega/k}\sqrt{\pi}\left[1+\mathrm{erf}\left(\frac{x}{2L}\right)\right]. \quad (17)$$

The perturbed distribution oscillates in phase with the electric field and is bounded. This is in contrast with the behavior of trapped equilibrium distributions, which are in phase with the wave potential (see e.g., Ref. 41). The amplitude of the oscillation increases monotonically through the packet; quite naturally, the amplitude vanishes for $x \ll -L$ and saturates for $x \gg L$, where the electric field is exponentially vanishing.

From Eqs. (13) and (17) we observe that the perturbed oscillating distribution f_e has, in general, components in and out of phase with respect to the electric field. The energy transfer between the waves and the electrons is due to the work done by the electric field on the perturbed electron current and is therefore carried by the in-phase, or resistive component of f_e. In order to clarify the transition between oscillation in and out of phase with the wave electric field, we rewrite (13) by splitting the oscillating contribution to f_e into resistive and reactive terms. The splitting emulates also the wave–correlator procedure

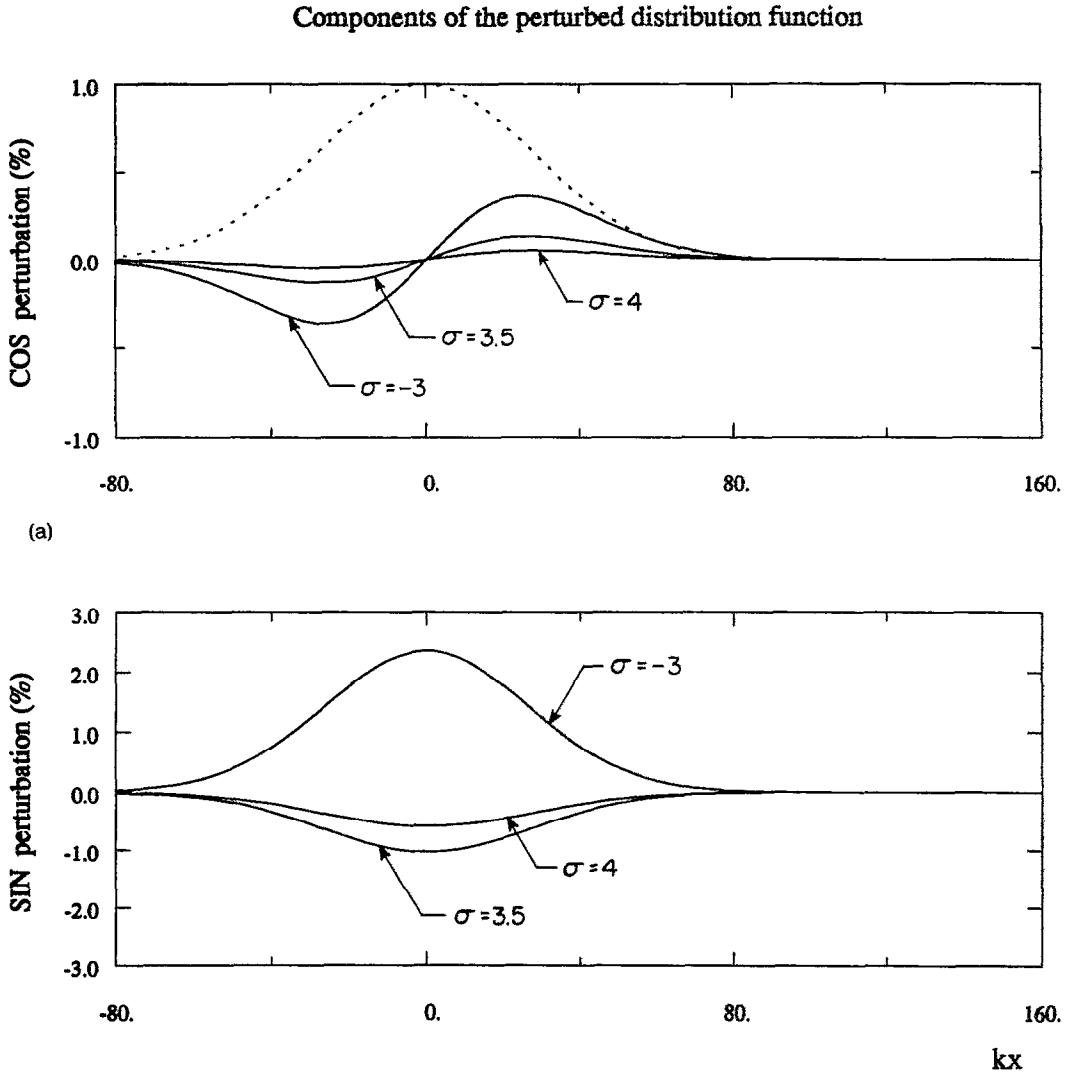

FIG. 2. (a) Linear perturbation $\hat{f}_e(x,v)$ with its two components: resistive (cos) and reactive (sin). The perturbation is shown as a function of position (wave number units) for three nonresonant velocities; $\sigma=(kv-\omega)L/v$. A dashed line indicates schematically the envelope of the wave electric field. The perturbation is spatially limited to the field region and is larger in the reactive component (note the different scales). Parameters: $\mu=0.2$, $kL=20$. (b) The same as (a), but for velocities close to or at resonance. The perturbations are much larger and extend downstream of the field region. The amplitude of the oscillation scales as $\exp(-\sigma^2)$, and its characteristic length is given by $L/\sigma=k^{-1}(1-v/v_p)^{-1}$. At resonant velocities, $\sigma\sim 0$, mainly the resistive component (cos) is strongly perturbed.

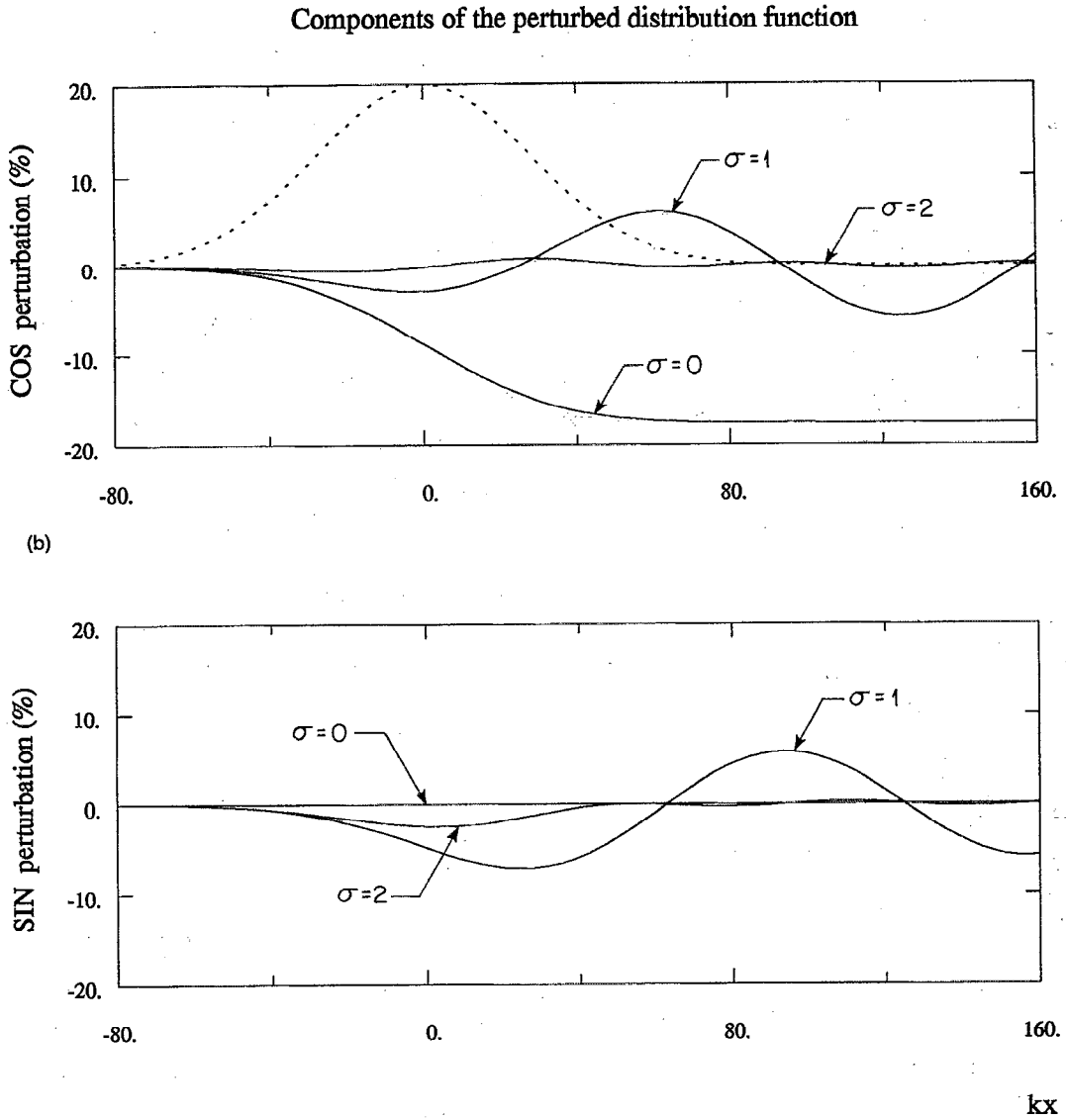

FIG. 2. (*Continued.*)

performed on rocket data.[13] Introducing the notation $\mu \equiv (2eE_0k/m)\ (kL/\omega)^2$, we obtain

$$\frac{f_e}{F_e} = \mu \frac{1}{kL} \frac{v_p^2}{v} \left(\frac{\partial}{\partial v} \ln F_e \right) \eta(x) [Z_i \cos(kx - \omega t) + Z_r \sin(kx - \omega t)]. \quad (18)$$

The factor μ may be thought of as the square of the bounce frequency in a constant amplitude field times the transit time of a resonant electron through the wave packet. It is similar to the left-hand side of (11). A validity condition for f_e being a solution to the Vlasov equation (2) is clearly $|\partial f_e/\partial v| \ll |\partial F_e/\partial v|$ inside the packet where E maximizes. Differentiating Eq. (13) and realizing that the strongest v dependence in f_e occurs via the variable ξ, it is straightforward to show that $|\partial f_e/\partial v| \simeq 2\mu |\partial F_e/\partial v|$ when evaluated at $v=v_p$ and $x=0$. Therefore, as long as $\mu \ll 1$, little nonlinear effect is expected to appear. Considering the parameters listed in Tables I and II, this inequality is satisfied. In the present analysis we use values up to $\mu \lesssim 0.2$, which for the aurora conditions corresponds to a packet of 80 m size and the rather large electric field of 500 mV/m.

Equation (18) shows that the perturbation is rather in or out of phase with the wave electric field, depending on the relative weight of Z_i and Z_r, imaginary and real parts of Z, respectively. For $\sigma=0$, e.g., Z is purely imaginary, which leads to Eq. (17). We split Eq. (18) into its resistive and reactive components $\hat{f}_c$ and $\hat{f}_s$: $(f_e/F_e) = \hat{f}_c \cos\psi + \hat{f}_s \sin\psi$. Figure 2 displays the components as a function of x for velocities far from resonance in panel (a) and for velocities close to resonance in panel (b). Here we have assumed a falling power law for the equilibrium distribution function of energetic electrons, $F_e = (v/v_p)^{-\alpha}$ with $\alpha=5$, and evaluated Eq. (18) numerically for $\mu=0.2$ and $kL=20$. To gain a qualitative understanding, it is useful to consider simple analytic limits to Eq. (18). Around the center of the packet, $|\chi| = |x/2L| < 1$, expanding Z gives the following approximate expressions. If $|\sigma|$ is large enough for $|\sigma + i\chi| > 2$,

$$\hat{f}_c \simeq \mu \frac{1}{kL} \frac{v_p^2}{v} \left(\frac{\partial}{\partial v} \ln F_e \right) \times \left(-\frac{\chi}{\sigma^2} e^{-\chi^2} + 2H(x) \sqrt{\pi}\, e^{-\sigma^2} \cos(2\sigma\chi) \right), \quad (19a)$$

$$\hat{f}_s \simeq \mu \frac{1}{kL} \frac{v_p^2}{v} \left(\frac{\partial}{\partial v} \ln F_e \right) \times \left(\frac{e^{-\chi^2}}{\sigma} + 2H(x) \sqrt{\pi}\, e^{-\sigma^2} \sin(2\sigma\chi) \right). \quad (19b)$$

Away from the center of the packet, $|\chi| > 1$, the expansion yields the approximate expressions,

$$\hat{f}_c \simeq \mu \frac{1}{kL} \frac{v_p^2}{v} \left(\frac{\partial}{\partial v} \ln F_e \right) \times \left(\frac{-\chi}{\chi^2+\sigma^2} e^{-\chi^2} + 2H(x) \sqrt{\pi}\, e^{-\sigma^2} \cos(2\sigma\chi) \right), \quad (20a)$$

$$\hat{f}_s \simeq \mu \frac{1}{kL} \frac{v_p^2}{v} \left(\frac{\partial}{\partial v} \ln F_e \right) \times \left(\frac{\sigma}{\chi^2+\sigma^2} e^{-\chi^2} + 2H(x) \sqrt{\pi}\, e^{-\sigma^2} \sin(2\sigma\chi) \right). \quad (20b)$$

The expressions above point out that for $|\sigma| > 2$, when $e^{-\sigma^2}$ is negligibly small, the perturbation is mainly in the sin term $\hat{f}_s$ and is confined to the region occupied by the

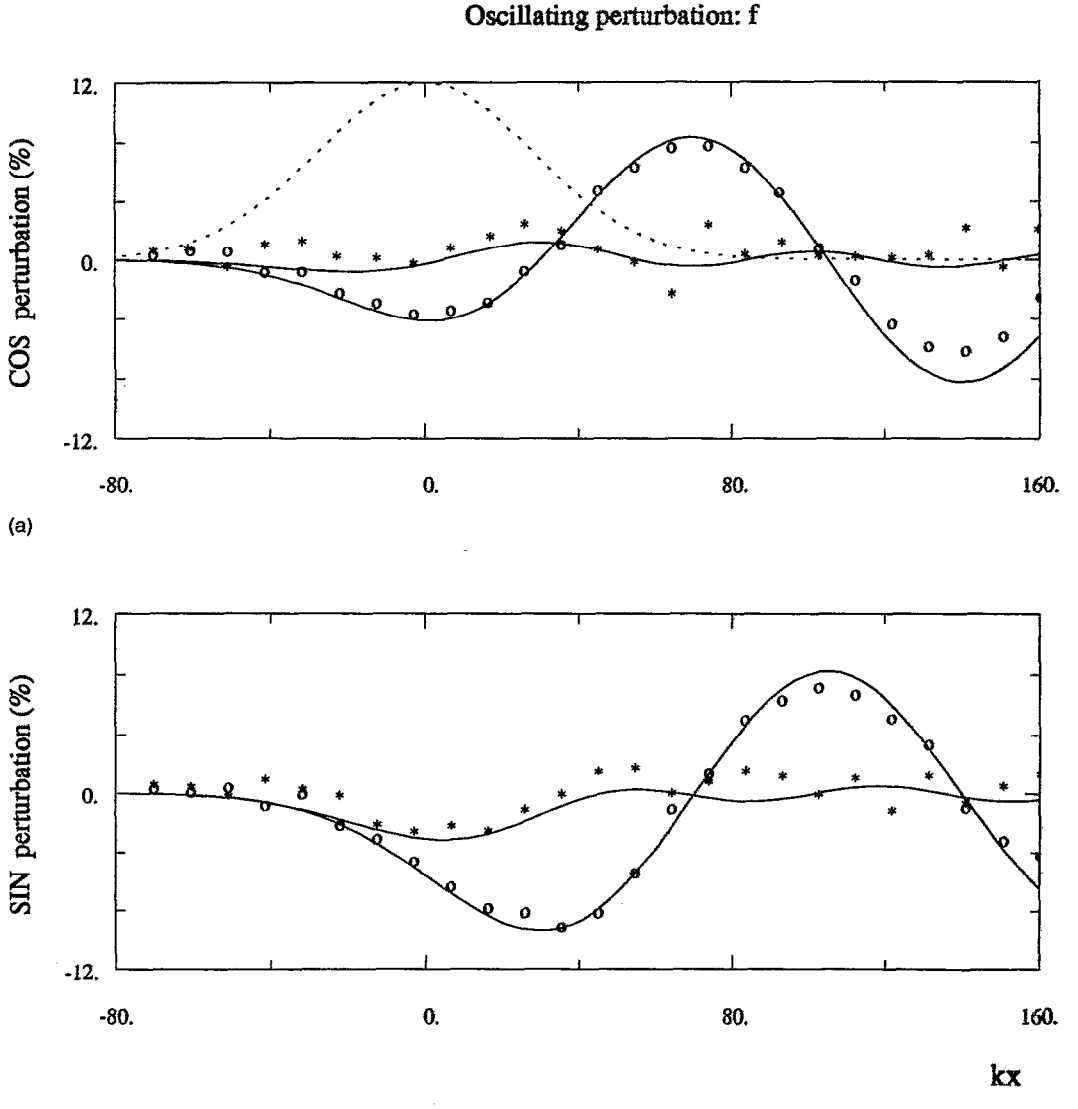

FIG. 3. (a) Amplitude of the perturbations in f observed in a test-particle simulation. The location of the electric field is indicated schematically with a dashed line. Two values of velocity are chosen: $\sigma=0.99$ (circles) and $\sigma=1.9$ (asterisks). The solid lines display the analytical results as described by f_e/F_e from Eq. (18). For $\sigma=1.9$, the amplitude of the bunching is too small, so that the data from the simulation are degraded by numerical noise. (b) The same as (a) for two other velocities: $\sigma=-1.1$ (circles) and $\sigma=0.02$ (asterisks). For resonant electrons ($\sigma=0.02$) the linear, resistive perturbation is large: $f_e/F_e \simeq 20\%$. The effect of nonlinear corrections from Ref. 21 is shown with a dot–dash pattern.

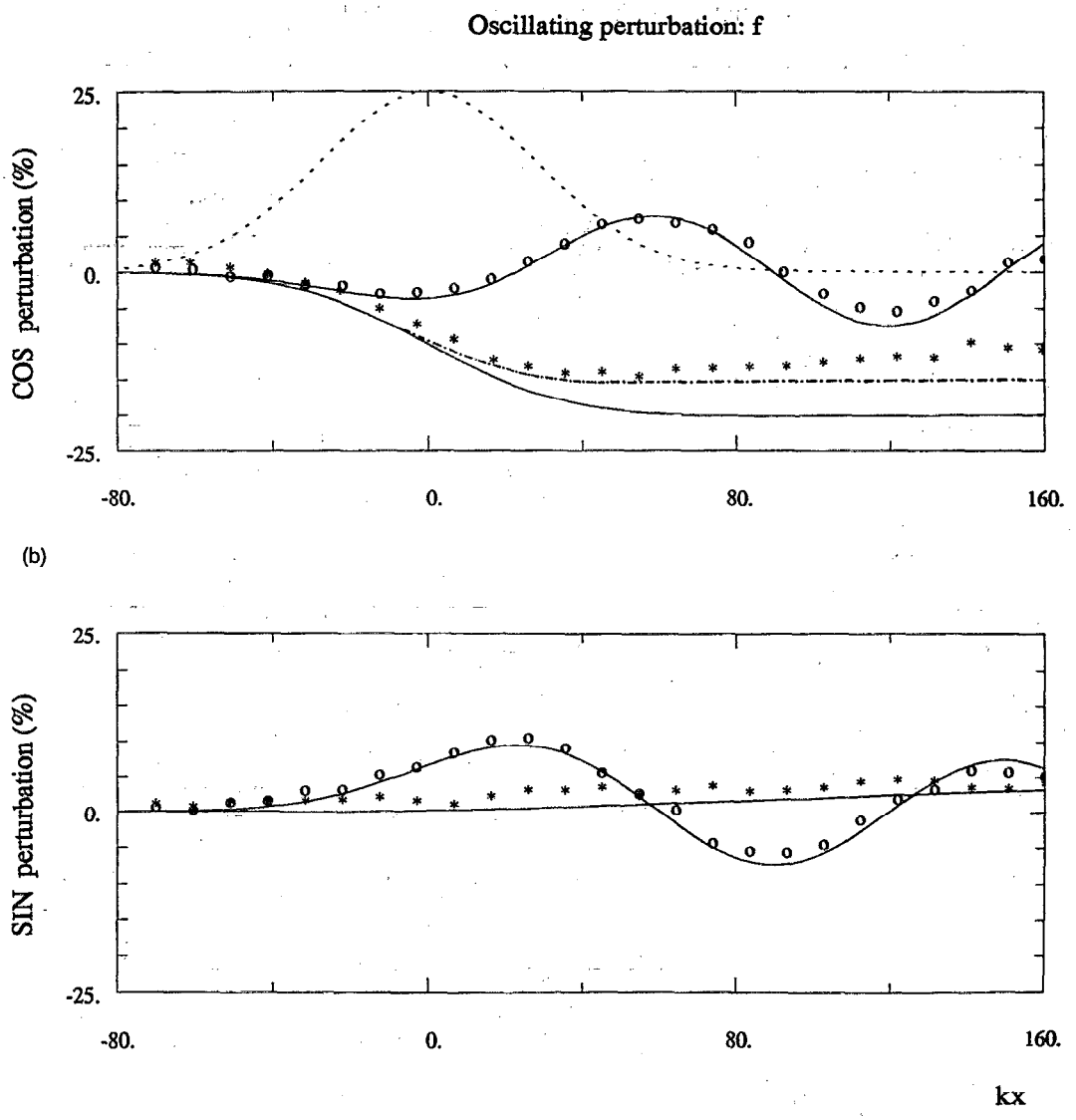

FIG. 3. (*Continued.*)

packet. Figure 2(a) shows exactly this behavior. The nonvanishing contribution is limited to the packet, whose envelope is indicated by a dashed line. Furthermore, $\hat{f}_s$ has the sign opposite to σ, in agreement with (19b), while $\hat{f}_c$ is odd in x, as described by (19a). On the other hand, when $|\sigma|<2$, the term $\exp(-\sigma^2)$ in Eqs. (20a) and (20b) becomes significant. The perturbed distribution sustains spatial oscillations with a wavelength $2\pi L/\sigma = (2\pi/k)(1-v/v_p)^{-1}$ in both reactive and resistive components for the whole downstream region ($x>0$). This behavior is displayed in Fig. 2(b). It appears clearly for $\sigma=1$, where $\hat{f}_c$ and $\hat{f}_s$ oscillates with a 10% amplitude and a wavelength $2\pi kL/\sigma=120$. For almost exactly resonant electrons, $\sigma\sim 0$ in Eqs. (20a) and (20b), $\hat{f}_s$ is vanishingly small, whereas $\hat{f}_c$ is large, negative, and nearly constant.

The presence of ballistic terms is well known in the Vlasov theory of wave–particle interactions. In Ref. 20, e.g., an expression like (20) is given for the perturbation downstream of a localized wave packet. Their reality has been strikingly demonstrated in laboratory plasmas by experiments on echo phenomena.[24,29,30]

Figure 3 compares Eq. (18) with results from a test-particle simulation code. In the simulation 500 000 electrons are launched through a given electrostatic wave packet. They are distributed both over a range of velocities around v_p and uniformly over the possible phases relative to the electric field. Their subsequent bunching in the phase of the wave field is analyzed with diagnostics which resemble the rocket-borne wave–electron correlator.[13] To simulate conditions in the aurora, we choose the packet to have a maximum amplitude of 500 mV/m and a half-width $L=20k^{-1}=40$ m. This choice corresponds to $\mu=0.23$ and, therefore, is at the boundary of the linear regime.

Figure 3(a) shows the perturbations as a function of position at two velocities: $v=1.85\times 10^9$ cm/s and $v=1.94\times 10^9$ cm/s, while the phase velocity is $v_p=1.76\times 10^9$ cm/s. We see a good fit between the two

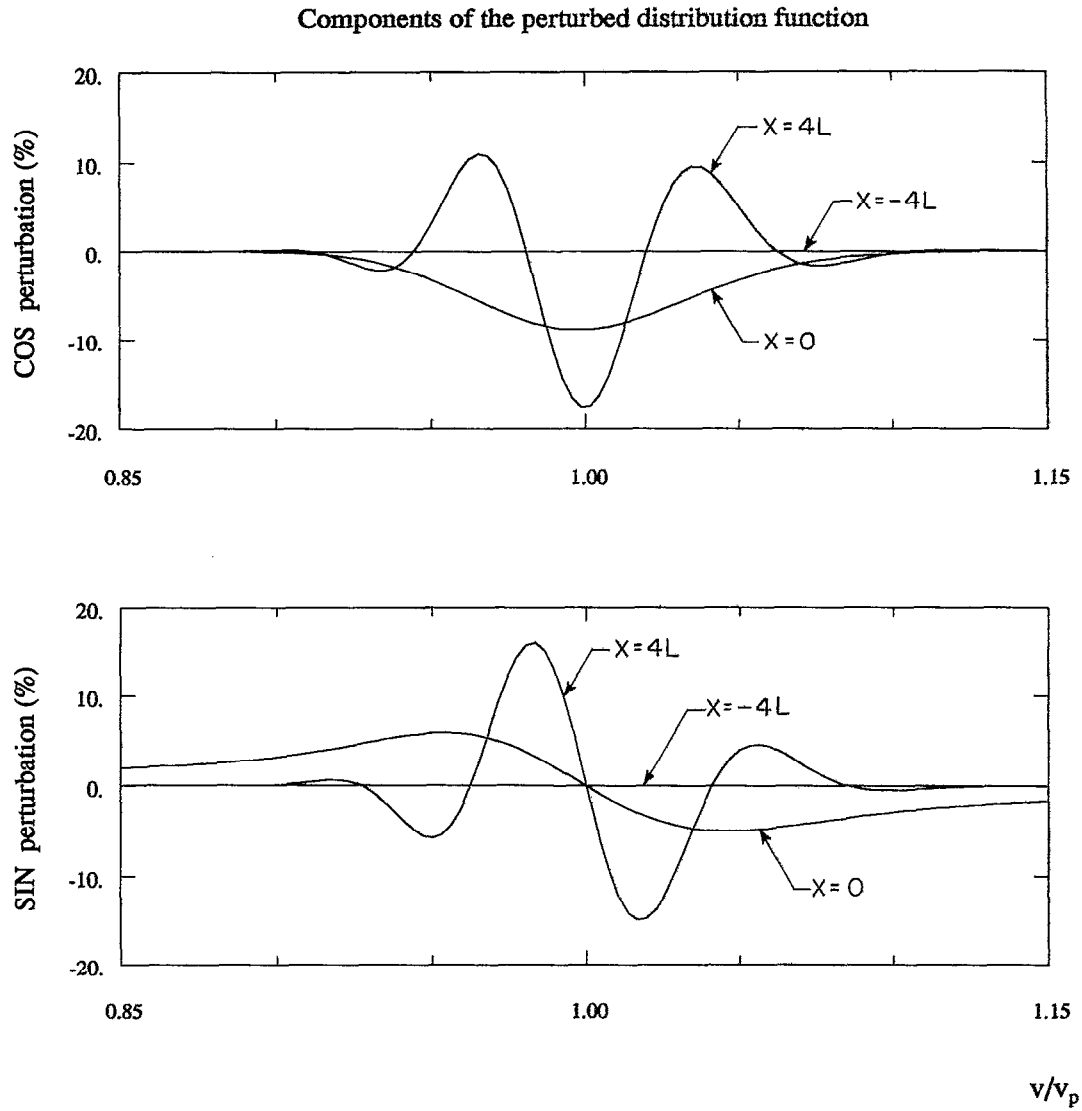

FIG. 4. Linear perturbation $\hat{f}_e(x,v)$ with its two components: resistive (cos) and reactive (sin). The perturbation is shown as a function of velocity (in units of the phase velocity v_p) for three locations: upstream ($x=-4L$), within ($x=0$), and downstream ($x=4L$) of the wave packet. The resistive component extends over the resonance interval $\Delta v=2v_p/(kL)$ on each side of v_p. Parameters: $\mu=0.2$, $kL=20$.

methods. As compared to the analytical Vlasov approach, the correlator-simulation method suffers from finite size velocity bins and from numerical noise, as well as from errors in diagnostics due to a required linear interpolation from electron position to the plotted position. On the other hand, it automatically includes any nonlinearity in the particle trajectory. Figure 3(b) depicts the comparison at velocities $v=1.67\times10^9$ cm/s and $v=1.76\times10^9$ cm/s, showing a remarkable fit between the two approaches. For the resonant particle ($\sigma=0.02$) the perturbation of the trajectory is large enough for nonlinear effects to play a role, and causes a small divergence between the results of each method. A dot–dash pattern indicates the result of the nonlinear calculation presented in Ref. 21. Still, the validity of the linear calculation is remarkable.

We conclude this section by showing a perturbed distribution as a function of velocity at several locations (Fig. 4). While at $x=-4L$ no effects are observed, we note for $x>0$ an oscillating behavior. From Eqs. (20) this behavior is due to the ballistic term $\exp(2i\sigma\chi)$. As $\chi=x/(2L)$ increases, the oscillation in σ (thus in v) increases. The electrons carry with them the memory of their interaction with the wave field after exiting the packet. However, for $x\gg L$ moments of f_e, like the density perturbation, do vanish because f_e oscillates in v. The resistive component $\hat{f}_c$ is approximately symmetric with respect to the phase velocity, while the reactive perturbation $\hat{f}_s$ is asymmetric. Therefore, the important lowest moment of f_e is associated to $\hat{f}_c$, which constitutes a source in the wave equation (8). This quantity is related to growth rates and changes in the wave profile, as will be discussed in the next section.

IV. WAVE PACKET EVOLUTION AND ENERGY EXCHANGE WITH RESONANT ELECTRONS

In the previous section, a stationary profile of the electric field has been assumed. The resulting linear perturbation in the distribution function just oscillates in time with frequency ω, the components $\hat{f}_c$ and $\hat{f}_s$ being in phase and out of phase with the electric field, respectively. The spatial behavior and amplitude of the perturbation was shown to agree well with the correlator function from test-particle simulations, which also assume a stationary electric field amplitude. In reality, the electron current resulting from the perturbed distribution function feeds back on the electric field. The current associated with the resistive component $\hat{f}_c$ extracts or deposits, after many wave periods, a non-negligible amount of the wave energy. This energy, which is tapped from or goes into the flux of passing electrons, modifies the wave profile in the course of time. In this section we analyze the effect of the passing electrons upon a localized electric field on the basis of Eq. (8). In the frame moving with velocity u the envelope experiences slow time changes driven by the resistive component n_c of the perturbed density.

For the applications we consider, we recall that the transit time of resonant electrons through the packet is of the order of tens to a hundred plasma periods (see Table II). The growth or damping time, on the other hand, is estimated from observations to be of order $\gamma^{-1}\sim 10^4\omega_p^{-1}$. It is therefore legitimate to consider the field as prescribed while solving the Vlasov equation for $f_e(x,v,t)$. Changing the coordinates to the moving frame: $x\to x-ut$, $v\to v-u$, $\omega\to\omega-ku$, and choosing the Gaussian shape defined in Eq. (12) leads to

$$f_e(x,v,t)=A_0\eta(x,t)e^{i(kx-\omega t)}\frac{\partial F_0}{\partial v}\frac{L}{v}\frac{1}{i}Z(-\sigma,-\chi)+\text{c.c.} \tag{21}$$

Compared to (13), the expression is written in the moving frame, and we have added an additional slow time dependence in η. The linear perturbation adiabatically follows the growth in the electric field, and has an amplitude and phase depending on Z, whose argument is explicitly split into its real and imaginary parts [as defined in (14)]. The real part, $-\sigma=(\omega-kv)L/v$, is unchanged from the stationary case: The Doppler-shifted frequency seen by the passing electron is not modified by the growth of the packet. The imaginary part, $-\chi=-x/(2L)$, reflects the spatial variation in amplitude of the electric field, as seen by the passing electron. It too is not modified because the amplitude of the packet hardly changes during the electron transit.

We seek now to calculate explicitly n_c by integrating Eq. (21) for f_e over velocities. Extracting the resistive component, we have

$$n_c(x,t)=-2A_0\eta(x,t)\frac{k}{\omega^2}\mathrm{Re}(\tilde{n}) \tag{22a}$$

where

$$\tilde{n}(x)=kLv_p^2\int dv\,\frac{1}{v}\frac{\partial F_e}{\partial v}iZ\left[L\left(\frac{\omega}{v}-k\right),-\frac{x}{2L}\right]. \tag{22b}$$

From Fig. 4, one sees that the resistive perturbation in $\hat{f}_e$ is confined to an interval $\Delta v=2v_p/(kL)$ on each side of the phase velocity. To compute $\mathrm{Re}(\tilde{n})$ amounts to averaging the slope of $F_e(v)$ with $(L/v)Z_i$ as a weighting function. This averaging and therefore the evolution of the wave packet depend strongly on the packet size kL.

For a very broad packet, $(L/v)Z_i$ is described by a Gaussian centered on v_p which mimics a delta function [see Fig. 1(a)], so that one obtains

$$\mathrm{Re}(\tilde{n})=-\pi\frac{\omega^2}{k^2}\frac{\partial F_e}{\partial v}\bigg|_{v_p}, \tag{23}$$

and the right-hand side of the wave equation (8) becomes

$$\mathrm{RHS}(8)=\frac{\omega_p^2}{k^2}\frac{\partial F_e}{\partial v}\bigg|_{v_p}\pi\left(\frac{\partial\epsilon}{\partial\omega}\right)^{-1}2A_0\eta.$$

In the moving frame the field amplitude varies exponentially with time, and the growth rate is given by

$$\gamma=\pi\frac{\omega_p^2}{k^2}\frac{\partial F_e}{\partial v}\bigg|_{v_p}\left(\frac{\partial\epsilon}{\partial\omega}\right)^{-1}. \tag{24}$$

Thus the familiar expression for a plane wave is recovered. The amplitude increases or decreases depending upon the slope of the nonoscillating distribution function of energetic electrons evaluated at v_p.

When kL is finite, on the other hand, the Gaussian centered on v_p that describes the response function broadens, as demonstrated in Fig. 1(a). Two situations may occur. Either the slope of $F_e(v)$ changes significantly, and even turns from positive to negative over the velocity interval $4v_p/(kL)$, or it remains fairly constant. First let us analyze the latter case, or packets satisfying the rough criterion,

$$kL>4v_p/\Delta v_+, \tag{25}$$

where Δv_+ is the range of velocities over which $\partial F_e/\partial v$ is positive. The integral in Eq. (22b) can be approximated by

$$\tilde{n}(x)=-v_p^2\frac{\partial F_e}{\partial v}\bigg|_{v_p}\int_C d\xi\,iZ(\xi), \tag{26}$$

in which the complex integration variable $\xi\equiv L(\omega/v-k)-ix/(2L)$ is introduced. The integration contour C is a horizontal segment running from $\mathrm{Re}\,\xi=kL\,\Delta v/(v_p-\Delta v)$ to $\mathrm{Re}\,\xi=kL\,\Delta v/(v_p+\Delta v)$. Even with those simplifications, the integral remains tedious to evaluate. As is shown in the Appendix, we obtain

$$\mathrm{Re}[\tilde{n}(x)]=-v_p^2\frac{\partial F_e}{\partial v}\bigg|_{v_p}\pi h\left(\frac{x}{2L}\right),$$

where

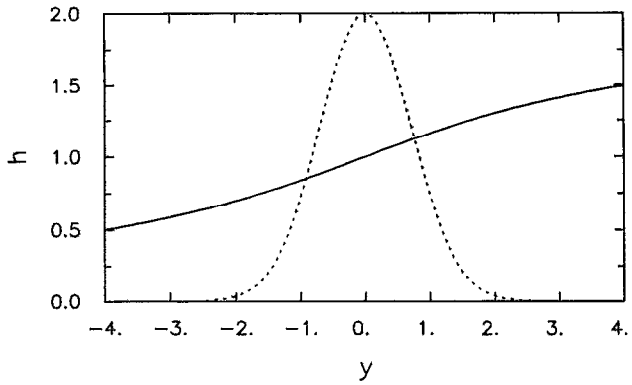

FIG. 5. Auxiliary function $h(y)$ defined by Eq. (27) and spatial profile of the wave field (dashed line with $y=x/2L$ and arbitrary amplitude).

$$h(y)=1+\operatorname{erf} y-\frac{1}{2\pi y}(1-e^{-y^2})+\frac{y}{\pi}\sum_{n>0}\frac{1}{n^2+4y^2}\left[4\exp\left(-y^2-\frac{n^2}{4}\right)-2-\operatorname{erf}\left(L_1-\frac{n}{2}\right)-\operatorname{erf}\left(L_2-\frac{n}{2}\right)\right], \tag{27}$$

and L_1, L_2 equal $2kL(kL-2)^{-1}$, $2kL(kL+2)^{-1}$, respectively. The function $h(y)$ describes the difference between the profiles of the perturbed density and the electric field. The asymmetry between positive and negative $y=x/(2L)$ reflects the increasing amplitude of the perturbed distribution as the electrons penetrate further into the wave packet. It is reminiscent of Eq. (17). A plot of $h(y)$ is displayed in Fig. 5: the function is monotonously increasing, is equal to unity at the center of the packet, and $h(y)-1$ is odd in y. Note, though, that the density itself vanishes where the field vanishes [Eq. (22a)], since $h(y)$ varies much slower than the envelope of the electric field, $\exp(-y^2)$, shown here in arbitrary units with a dotted line. Substituting $\mathrm{Re}(\tilde{n})$ in Eq. (22a) gives the spatial distribution of the perturbed density,

$$n_c(x)=2A_0\frac{1}{k}\frac{\partial F_e}{\partial v}\bigg|_{v_p}\pi\eta(x,t)h\left(\frac{x}{2L}\right). \tag{28}$$

Thus the wave equation can be written as

$$\frac{\partial\eta}{\partial t}=\gamma h\left(\frac{x}{2L}\right)\eta, \tag{29}$$

with γ defined in Eq. (24). Since, as noted above, $h(x/2L)$ is slowly varying compared to $\eta(x)$, we expand it to first order $h(x<L)\cong 1+x/(12L)$. That leads to

$$\eta(x,t)=\exp\left\{-\left[\frac{x}{2L}-\left(\frac{u}{2L}+\frac{\gamma}{12}\right)t\right]^2\right\}\times\exp\left[\gamma t\left(1+\frac{\gamma t}{144}\right)\right], \tag{30}$$

in which the group velocity u has been reintroduced. For several exponentiations the packet maintains its Gaussian shape while slowly drifting. A similar result was demonstrated in a different context by means of a saddle-point method[39,42] and shown in a particle simulation [see Fig. 1(a) in Ref. 18].

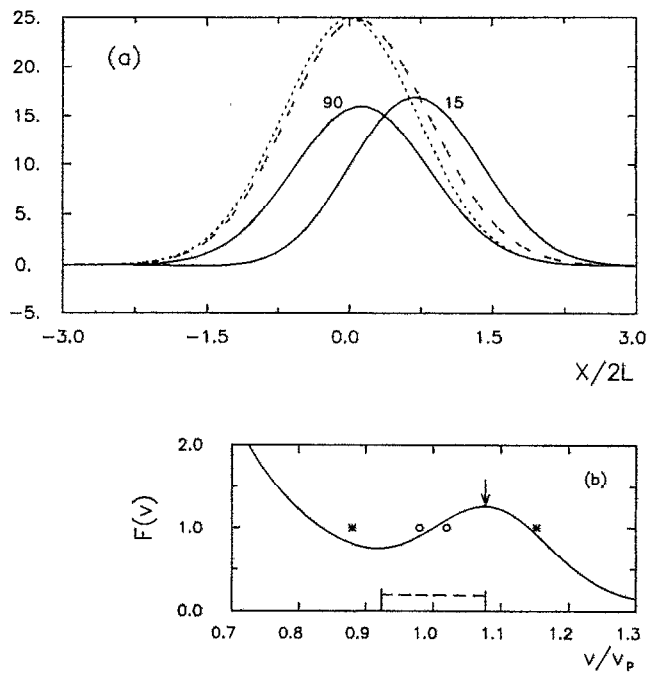

FIG. 6. (a) Spatial profiles of the source term for the wave envelope equation (8) and inferred change in the envelope. (b) Model distribution function $F(v)$ around the phase velocity v_p (the position of the beam velocity v_b and the range Δv_+ are indicated by an arrow and a dashed line, respectively). For a broad packet ($kL=90$), the profile is nearly centered [the solid curve labeled 90 in panel (a)], while its resonant velocity interval comprises a narrow range of positive slopes [delimited by the two circles in (b)]. For a narrow packet ($kL=15$), the velocity interval includes positive and negative slopes [asterisks in (b)] and the spatial profile is shifted downstream. This widens the field envelope [dashed versus dotted curves in (a)].

This "self-similar" growth or decay of the packet occurs where $\mu\ll 1$, namely the resonant electrons have no time to bounce. On the other hand, where $\mu=0$ (1) trapping and transit times are of the same order, so that nonlinear effects can be expected.[25] The damping of an intense wave packet was investigated by Denavit and Sudan.[18] It was shown that the wave field becomes broader with the formation of several new lobes. In the case of growth, nonlinear effects reverse the sign of the resistive perturbed density on the downstream side of the packet.[20] This might, on the contrary, lead to an enhanced localization of the wave field.[21]

We return now to Eqs. (22) and consider compact packets satisfying the inequality opposite to (25). The slope of $F_e(v)$ turns from positive to negative over the resonant velocity interval. A model of such a local distribution function is shown in Fig. 6(b) (in normalized units). It is made of a Gaussian bump added to a falling power law; the slope at $v=v_p$ is equal to 5 and $\Delta v_+=0.15v_p$. For that $F_e(v)$ we integrate Eq. (22b) numerically and display the result in Fig. 6(a). The quantity $\eta\,\mathrm{Re}(\tilde{n})$, which represents the spatial profile of the source

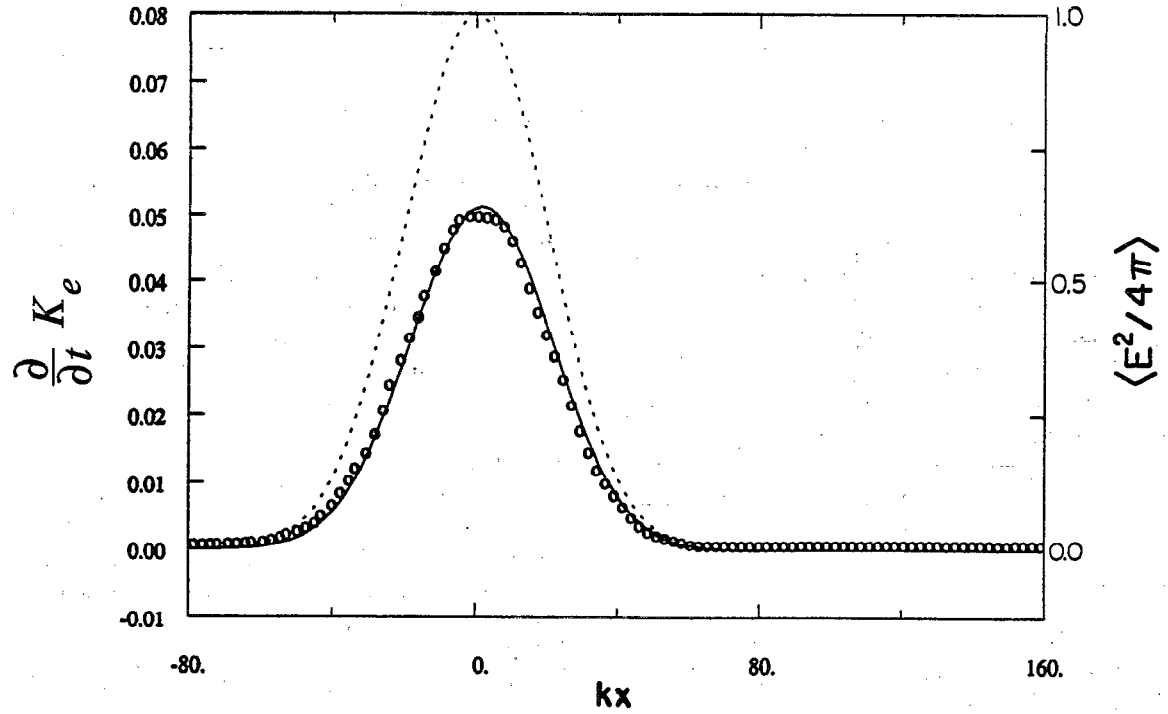

FIG. 7. Energy exchange observed in a test-particle simulation. Case of wave damping, where $\gamma = -2.5 \times 10^{-4}\ \omega_p$. Left scale: rate of energy deposition into resonant electrons from the simulation (circles) and from theory (solid line), in $\omega^2(\partial\epsilon/\partial\omega)E_0^2/4\pi$ units. Right scale: profile of the field energy in arbitrary units (dashed line).

term for Eq. (8), is shown (solid lines) for two packet widths as a function of normalized position. The labels denote the value of kL for each packet. For $kL=15$ the resonant velocity interval, indicated by two asterisks in panel (b), is broader than Δv_+ and satisfies the reverse inequality to (25). The source term appears totally shifted with respect to the packet center. To understand the spatial behavior of n_c, it is useful to consider Fig. 4(a), in which the resistive component reflects the behavior of $-v^{-1}Z_i \exp(-\chi^2)$ with v at various positions. For $x \leqslant 0$, Z_i has a constant positive sign, so the slope of $F_e(v)$ averaged over the resonant velocity interval is reduced from the value $(+5)$ it has at $v=v_p$. As a result, little energy is deposited by the passing electrons into the wave field on the upstream side. For $x>0$, on the other hand, the ballistic term $\exp(-\sigma^2)\cos(2\sigma\chi)$ causes Z_i to oscillate and change sign over the resonant velocity interval. The first zeros on the v axis around v_p are given by $(1-v_p/v) = \pm\pi/2(kx)^{-1}$. Hence, there exists an optimum position x_0 for which the sign change of Z_i is synchronized with that of the slope of F_e. Negative slopes are given a "negative weight" in the averaging, which results in a large positive growth. This occurs for

$$\frac{x_0}{2L} = \frac{\pi}{2}\frac{v_p}{\Delta v_+}(kL)^{-1}$$

and causes the surge about $x=1.5L$ in Fig. 6(a). The effect upon the field envelope η is indicated by dotted and dashed lines. The renormalized envelope (dashed) is wider than the original envelope (dotted). Unlike broad wave packets, which experience the "self-similar" growth discussed above, narrow packets widen rapidly until $kL\,\Delta v_+/v_p \approx 4$, at which value the factor $\exp(-\sigma^2)$ drastically reduces the ballistic term, thus suppressing the anomalous contribution of negative slopes to wave growth. We emphasize that the widening takes place on a kinetic time scale, which is of order $\gamma^{-1} < 10^4\omega_p^{-1}$, therefore faster than the usual dispersion time $\tau_d \sim (kL)^2(v_p/v_t)^2\omega_p^{-1} > 10^5\omega_p^{-1}$. Since in space plasmas Δv_+ is upper bounded, the process sets a natural lower bound to the sizes of packets to be observed. If a narrower packet happens to be measured, it must be the product of a complex, nonlinear evolution that has decoupled the waves from the beam. It is clear that the exact bound depends on the details of the distribution function. Using the parameters in Table I, however, we note that Eq. (25) gives a minimum size, $kL \approx 20$, which is not far from the smallest packets observed in the aurora. The second curve in Fig. 6(a) represents the source term in case of a broad packet with $kL=90$. The slope hardly changes over the resonant velocity interval, indicated by two circles in panel (b), so that one recovers the "self-similar" growth described by Eq. (30). In accord with Eq. (23) the height at $x=0$ is given by $\pi\,\partial F_e/\partial v = 16$.

We wish now to compare the prediction of Eq. (29) to our test-particle simulations. In those simulations we have access to the kinetic energy of the resonant electrons $K_e(x,t)$. Choosing a falling power law for $F_e(v)$, the wave total energy (electric and mechanic) is expected to decrease while K_e increases. The rate of energy deposited into resonant electrons is thus computed and compared to

$$\frac{\partial}{\partial t}K_e=-\omega\frac{\partial\epsilon}{\partial\omega}\frac{E_0^2}{4\pi}\frac{\partial}{\partial t}\eta^2=-\frac{\omega}{2}\frac{\omega_p^2\partial F_e}{k^2\,\partial v}\bigg|_{v_p}E_0^2\eta^2h, \qquad (31)$$

where Eqs. (29) and (24) have been used. The solid line in Fig. 7 indicates the result of (31) while the circles show the simulation result. For comparison, the dashed line represents the wave energy profile η^2. Note the slight shift to the right, which is due to the asymmetry in the perturbed electrons with respect to the center of the packet and is described by the function h.

With a relationship similar to (22a) the reactive component n_s of the perturbed density is proportional to the imaginary part of $\tilde{n}$. On the basis of Fig. 1(b), one can see that the latter depends on the derivative of $\partial F_e/\partial v$ at v_p. More specifically, expanding $\partial F_e/\partial v$ and using Eq. (15) yields $\mathrm{Im}(\tilde{n})\sim v_p^3(\partial^2F_e/\partial v^2)(kL)^{-1}$. Therefore, the reactive to resistive ratio of components scales as

$$\frac{n_s}{n_c}\sim v_p\left(\frac{\partial}{\partial v}\ln\left|\frac{\partial F_e}{\partial v}\right|\right)_{v_p}(kL)^{-1},$$

and vanishes in the limit of a plane wave. That is consistent with Eq. (5a) giving the dispersion relation. For a compact packet though, a curvature of F_e about v_p leads to a differential growth among the packet Fourier components, $d\gamma/dk\neq0$, which results in a drift of the central wave number.[39] Here, however, considering the relation between n_c and γ, one readily shows that the right-hand side of Eq. (5a) behaves in magnitude as

$$\mathrm{RHS(5a)}\sim\frac{n_s}{n_c}\frac{\gamma}{\omega}(A_0\eta k).$$

It is several orders smaller than the first term in (5a), and so was rightly neglected.

From an experimental viewpoint, the growth rate can be evaluated by integrating the perturbed density as we did with Eq. (28). The integration of the resistive component of the perturbed distribution function is performed electronically onboard the satellite, directly from the measured correlator data. This procedure allows us to assess a growth rate without having to rely on the too often uncertain measurements of positive slope in the reduced distribution function. The technique shall be used onboard the Fast Auroral SnapshoT (FAST) satellite.[15]

V. CONCLUSIONS AND SUMMARY

Phase correlation between waves and particles is an important tool for the understanding of the kinetic interaction between localized waves and streaming electrons. In this paper we have analyzed the interaction between streaming, energetic electrons and a packet of Langmuir waves. The analysis is motivated by observations of Langmuir waves in the solar wind and on low-altitude auroral field lines, which frequently indicate that the high-frequency wave power is concentrated in spatially localized electrostatic packets whose dimensions are small enough ($kL\sim$10–100) to significantly affect the character of the wave–particle interaction. Our aim has been to address the following questions: (1) What is the effect of localized Langmuir waves on the bunching of electrons in phase space? (2) How do the perturbations of the electron distribution function affect the evolution of the Langmuir waveform? (3) What are the parameters that control these processes?

It is essential that resonant electrons have only a short transit time of 10–100 plasma periods to interact with the wave. The finite transit time has several important consequences. First, even resonant electrons, which are mostly susceptible to trajectory deformation, may have their orbits only slightly perturbed. Second, during this short interaction time the packet is considered as coherent, an assumption supported by the experimental success of the wave–electron correlator in the auroral zone.[13] Additionally, the wave field encountered by the passing electrons can be considered as prescribed. Thus, our investigation has been carried out by analytically integrating the Vlasov equation through a localized, coherent wave packet of a given amplitude and form factor. The finite interaction time is reflected in the frequency domain by a broadening of the Čerenkov resonance at $\omega=kv$. Besides, due to the short transit time the singularity in the linearly perturbed distribution function at resonance is removed. For a localized packet with a Gaussian envelope, the resistive component of the resonance function is a Gaussian in velocity space centered at the phase velocity. Its height and width are given by kL and $1/kL$, respectively. For finite kL values, a non-negligible broadening of the resonant velocity takes place, $\Delta v=2v_p/(kL)$. On the other hand, for very large values of kL, the resonant function mimics the delta function associated with a plane wave.

The important parameter that measures the effect of the localized wave field on the electrons is $\mu\equiv(2eE_0k/m)(kL/\omega)^2$. It may be thought of as the square of the average bounce frequency times the transit duration of a resonant electron. As long as $\mu\ll1$, transiting electrons cannot exchange much energy with the field in the packet, and their orbits remain close to unperturbed trajectories. The amplitude of the linear perturbed distribution function of the streaming electrons f_e is such that their derivative $|\partial f_e/\partial v|$ is negligible versus the derivative of the unperturbed electrons $|\partial F_e/\partial v|$, so that nonlinear perturbations in the Vlasov equation can be ignored. This is confirmed by a remarkable agreement between the analytical results for f_e and the data from test-particle simulations. The linear perturbed distribution function $f_e(x,v,t)$ can be written explicitly by means of the plasma Z function with an argument that includes x and v dependencies (unlike the usual plasma dispersion function with normalized phase velocity). The asymmetry of Z with respect to changing the sign of the imaginary part of the argument reflects the asymmetry between "upstream" and "downstream" electrons. Depending upon the relative weight of Z_i and Z_r, the perturbation is rather resistive or reactive, a characteristic that can be measured by the wave–electron correlator.[13]

The important parameter that controls the interaction between the packet and electrons with various velocities v is $\sigma\equiv(kv-\omega)L/v$, the Doppler-shifted frequency times

the transit duration. It distinguishes resonant particles (for which $|\sigma|<1$) from nonresonant ones (with $|\sigma|>2$). For $|\sigma|>2$, the perturbation of the distribution function is small, mostly reactive, and spatially limited to the location of the wave electric field. For $|\sigma|<1$, the perturbation is large, mostly resistive, and "permanent" in the sense that it is carried downstream of the packet. It reaches the amplitude of about $|f/F_e|\approx 2\mu/(kL)v_p|\partial \ln F_e/\partial v|$. In between ($1<|\sigma|<2$), the perturbation occurs in both reactive and resistive components, and displays large spatial oscillations as remnants of the interaction.

As for the effect of the interaction on the wave packet itself, we have computed explicitly the resistive component of the perturbed density in order to find the spatial modifications in the wave field envelope. If the distribution function includes a bump superimposed to the nonthermal tail, there is a natural packet width that depends upon the detailed slope of $F_e(v)$ about v_p and is given by $kL=4v_p/\Delta v_+$. Narrower packets broaden rapidly while they grow. Larger packets grow "self-similarly," i.e., they preserve their shape. This sets a lower bound $(kL)_{\min}\approx 20$ to observed packet sizes.

The maximum phase bunching is predicted to occur for resonant particles and to be in phase with the electric field. This feature is actually consistent with the measurements[19] made in the auroral zone by the wave–electron correlator, and contrasts with trapped equilibrium distributions which are bunched in phase with the wave potential. The fact that bunching maximizes for resonant electrons enables one to assess the phase velocity, hence the wavelength of the Langmuir waves. Besides, the phase relation confirms the spatial localization of the Langmuir packets. Furthermore, the range of observed packet sizes has a lower end that is consistent with the bound $(kL)_{\min}$. New correlation experiments on board the Freja and FAST satellites are expected to help in better understanding the kinetic effects associated to Langmuir waves and energetic electrons in the auroral zone.[15,16] In particular, the wave growth rate will be assessed directly from the resistive component of the perturbed distribution function, avoiding thus uncertain measurements of positive slope in the reduced distribution function.

As a wave packet grows, the associated parameter μ increases exponentially (at a rate of approximately $10^{-4}\,\omega_p$). When $\mu\gtrsim 0.2$, the amplitude of the perturbed distribution function becomes such that nonlinear perturbations in the Vlasov equation must be accounted for. The resistive component of the nonlinear perturbed density alters the shape of the packet and leads to an enhanced localization in the wave profile, whereby an extended wave packet of small amplitude becomes a more intense packet of shorter extension.[21] This kinetic localization operates for relatively low wave amplitudes and may be important when the usual localization due to self-focusing by ponderomotive effect is weak.

ACKNOWLEDGMENTS

We are indebted to a referee for drawing our attention to the work done over 20 years ago on wave–particle interactions.

This work was supported in part by the National Aeronautics and Space Administration (NASA) Grant Nos. NAG6-10 and NAGW-1626 as well as Contract Nos. NAS5-30367, NAS5-30366, and NAS5-31283.

APPENDIX: INTEGRATION OF THE PERTURBED DENSITY

Details concerning the evaluation of the integral of Eq. (26) are given here. Throughout the appendix we use the dimensionless units: $x\to kx$, $v\to v/v_p$, $t\to\omega t$, and $F_0\to v_pF_0$. Thanks to the connection between the Z function and complex error function, the integral to evaluate reads as

$$\tilde{n}(x)=-\left.\frac{\partial F_0}{\partial v}\right|_{v=1}\int_C d\xi\, iZ(\xi)$$

$$=\frac{\partial F_0}{\partial v}\sqrt{\pi}\int_C d\xi\, e^{-\xi^2}[1+\mathrm{erf}(i\xi)]. \tag{A1}$$

The contour C is a horizontal segment in complex plane defined by

$$\xi=L\left(\frac{1}{v}-1\right)-i\frac{x}{2L},$$

where v varies from $1-\delta$ to $1+\delta$, δ being a small number compared to unity [from Fig. 4 we note that $\delta\approx 2(kL)^{-1}$ is large enough to encompass most of the perturbed $\hat{f}_c$]. The end points of the segment are given by $\xi_r=L_1=L\delta/(1-\delta)$ and $\xi_r=-L_2=-L\delta/(1+\delta)$. The first term in the rightmost member of (A1) gives merely

$$j_1=\frac{\pi}{2}\frac{\partial F_0}{\partial v}[-\mathrm{erf}(L_1+i\xi_i)+\mathrm{erf}(-L_2+i\xi_i)]. \tag{A2}$$

In order to evaluate the term left over,

$$j_2=\frac{\partial F_0}{\partial v}\sqrt{\pi}\int_C d\xi\, e^{-\xi^2}\,\mathrm{erf}(i\xi), \tag{A3}$$

we utilize the following series approximation to the complex error function (see formula 7.1.29 in Ref. 43):

$$\mathrm{erf}(-\xi_i+i\xi_r)=-\mathrm{erf}(\xi_i)-\frac{e^{-\xi_i^2}}{\pi}\sum_{n=-\infty}^{+\infty}\frac{e^{-n^2/4}}{n^2+4\xi_i^2}$$

$$\times\left(2\xi_i-\xi_i e^{i2\xi_i\xi_r}(e^{n\xi_r}+e^{-n\xi_r})\right.$$

$$\left.+\frac{in}{2}e^{i2\xi_i\xi_r}(e^{n\xi_r}-e^{-n\xi_r})\right).$$

Substituting this expression in (A3) and performing the integrals over ξ_r, one obtains

$$j_2=-j_1\left(\operatorname{erf}(\xi_i)+\frac{e^{-\xi_i^2}}{\pi}\sum_{n=-\infty}^{+\infty}2\xi_i\frac{e^{-n^2/4}}{n^2+4\xi_i^2}\right)-\frac{\partial F_0}{\partial v}\frac{1}{2}$$
$$\times\sum_{n=-\infty}^{+\infty}\frac{\xi_i}{n^2+4\xi_i^2}\left[\operatorname{erf}\left(L_1+\frac{n}{2}\right)+\operatorname{erf}\left(L_2-\frac{n}{2}\right)\right.$$
$$\left.+\operatorname{erf}\left(L_1-\frac{n}{2}\right)+\operatorname{erf}\left(L_2+\frac{n}{2}\right)\right]+\frac{\partial F_0}{\partial v}\frac{i}{2}$$
$$\times\sum_{n=-\infty}^{+\infty}\frac{n}{n^2+4\xi_i^2}\frac{1}{\sqrt{\pi}}\int_{L_1}^{-L_2}dy_r$$
$$\times(e^{-(y-n/2)^2}-e^{-(y+n/2)^2}). \tag{A4}$$

The term on the last line is purely imaginary and does not require evaluation, since we are interested in the real part of $\tilde{n}(x)=j_1+j_2$ only. Summing up all real terms and rearranging the sums over n, one obtains

$$\operatorname{Re}(\tilde{n})=\operatorname{Re}(j_1)\left(1-\operatorname{erf}(\xi_i)-\frac{e^{-\xi_i^2}}{2\pi\xi_i}\right.$$
$$\left.-\frac{e^{-\xi_i^2}}{\pi}4\xi_i\sum_{n>0}\frac{e^{-n^2/4}}{n^2+4\xi_i^2}\right)$$
$$-\frac{\partial F_0}{\partial v}\frac{1}{4\xi_i}[\operatorname{erf}(L_1)+\operatorname{erf}(L_2)]-\frac{\partial F_0}{\partial v}$$
$$\times\sum_{n>0}\frac{\xi_i}{n^2+4\xi_i^2}\left[\operatorname{erf}\left(L_1+\frac{n}{2}\right)+\operatorname{erf}\left(L_2+\frac{n}{2}\right)\right.$$
$$\left.+\operatorname{erf}\left(L_1-\frac{n}{2}\right)+\operatorname{erf}\left(L_2-\frac{n}{2}\right)\right]. \tag{A5}$$

Now a typical value for $L_\alpha(\alpha=1,2)$ is 2. This allows us to set $\operatorname{erf}(L_\alpha)=1$ and to approximate $\operatorname{Re}(j_1)$ by $-\pi\,\partial F_0/\partial v$. Thus (A5) results in

$$\operatorname{Re}(\tilde{n})=-\pi\frac{\partial F_0}{\partial v}h(-\xi_i),$$

with

$$h(y)\equiv 1+\operatorname{erf}(y)-\frac{1}{2\pi y}(1-e^{-y^2})$$
$$+\frac{y}{\pi}\sum_{n>0}\frac{1}{n^2+4y^2}\left[4\exp\left(-y^2-\frac{n^2}{4}\right)-2\right.$$
$$\left.-\operatorname{erf}\left(L_1-\frac{n}{2}\right)-\operatorname{erf}\left(L_2-\frac{n}{2}\right)\right].$$

[1] R. P. Lin, D. W. Potter, D. A. Gurnett, and F. L. Scarf, Astrophys. J. **251**, 364 (1981).
[2] D. A. Gurnett and R. R. Anderson, J. Geophys. Res. **82**, 632 (1977).
[3] D. B. Melrose, G. A. Dulk, and I. H. Cairns, Astron. Astrophys. **163**, 229 (1986).
[4] P. A. Robinson, I. H. Cairns, and D. A. Gurnett, Astrophys. J. Lett. **387**, L101 (1992).
[5] R. P. Lin, W. K. Levedahl, W. Lotko, D. A. Gurnett, and F. L. Scarf, Astrophys. J. **308**, 954 (1986).
[6] T. Takakura and H. Shibahashi, Sol. Phys. **46**, 323 (1976).
[7] G. R. Magelssen and D. F. Smith, Sol. Phys. **55**, 211 (1977).
[8] L. Muschietti, Sol. Phys. **130**, 201 (1990).
[9] L. Muschietti, M. V. Goldman, and D. Newman, Sol. Phys. **96**, 181 (1985).
[10] D. B. Melrose and M. V. Goldman, Sol. Phys. **107**, 329 (1987).
[11] P. A. Robinson, Sol. Phys. **139**, 147 (1992).
[12] J. P. McFadden, C. W. Carlson, and M. H. Boehm, J. Geophys. Res. **91**, 12 079 (1986).
[13] R. E. Ergun, C. W. Carlson, J. P. McFadden, J. H. Clemmons, and M. H. Boehm, J. Geophys. Res. **96**, 225 (1991).
[14] M. Temerin, J. McFadden, M. Boehm, C. W. Carlson, and W. Lotko, J. Geophys. Res. **91**, 5769 (1986); J. McFadden, C. W. Carlson, and M. Boehm, *ibid.* **92**, 11 133 (1987).
[15] M. Temerin, C. W. Carlson, C. A. Cattell, R. E. Ergun, J. P. McFadden, F. S. Mozer, D. M. Klumpar, W. K. Peterson, E. G. Shelly, and R. C. Elphic, in *Physics of Space Plasmas*, edited by T. Chang, G. B. Crew, and J. R. Jasperse (Scientific Publishers Inc., Cambridge, MA, 1990), p. 97.
[16] R. Lundin, *EOS Transactions, American Geophysical Union*, April Supplement, 1993, Vol. 74, p. 274.
[17] D. L. Newman, P. A. Robinson, and M. V. Goldman, Phys. Rev. Lett. **62**, 2132 (1989).
[18] J. Denavit and R. N. Sudan, Phys. Rev. Lett. **28**, 404 (1972).
[19] R. E. Ergun, C. W. Carlson, J. P. McFadden, D. M. TonThat, J. H. Clemmons, and M. H. Boehm, J. Geophys. Res. **96**, 11 371 (1991).
[20] D. Nunn, J. Plasma Phys. **5**, 199 (1971).
[21] L. Muschietti, I. Roth, and R. E. Ergun, in Ref. 16, p. 266.
[22] L. Landau, J. Phys. USSR **10**, 25 (1946).
[23] T. M. O'Neil and R. W. Gould, Phys. Fluids **11**, 134 (1968).
[24] J. H. Malmberg, C. B. Wharton, R. W. Gould, and T. M. O'Neil, Phys. Fluids **11**, 1147 (1968).
[25] T. M. O'Neil, Phys. Fluids **8**, 2255 (1965).
[26] J. H. Malmberg and C. B. Wharton, Phys. Rev. Lett. **19**, 775 (1967).
[27] C. B. Wharton, J. H. Malmberg, and T. M. O'Neil, Phys Fluids **11**, 1761 (1968).
[28] M. V. Goldman, Phys. Fluids **13**, 1281 (1970); M. V. Goldman and H. L. Berk, *ibid.* **14**, 801 (1971).
[29] G. J. Morales and J. H. Malmberg, Phys. Fluids **17**, 609 (1974).
[30] F. Gervais, J. Olivain, A. Quemeneur, and M. Trocheris, Phys. Fluids **23**, 2034 (1980).
[31] P. A. Robinson, Phys. Fluids B **1**, 490 (1989); A. Y. Wong, P. Leung, and D. Eggleston, Phys. Rev. Lett. **39**, 1407 (1977).
[32] G. J. Morales and Y. C. Lee, Phys. Rev. Lett. **33**, 1534 (1974).
[33] D. B. Melrose and N. F. Cramer, Sol. Phys. **123**, 343 (1989).
[34] R. J.-M. Grognard, Sol. Phys. **81**, 173 (1982).
[35] P. A. Robinson, Phys. Fluids B **3**, 545 (1991).
[36] G. Pelletier, Phys. Rev. Lett. **49**, 782 (1982).
[37] P. A. Robinson and D. L. Newman, Phys. Fluids B **2**, 3120 (1990).
[38] D. Levron, G. Benford, A. B.-A. Baranga, and J. Means, Phys. Fluids B **1**, 2026 (1988); A. Dovrat and G. Benford, *ibid.* **1**, 2488 (1989).
[39] L. Muschietti and C. T. Dum, Phys. Fluids B **5**, 1383 (1993).
[40] C. T. Dum and T. H. Dupree, Phys. Fluids **13**, 2064 (1970).
[41] T. H. Stix, *Waves in Plasmas* (American Institute of Physics, New York, 1992), p. 160.
[42] M. Tanaka, M. Fugiwara, and H. Ikegami, Phys. Rev. A **34**, 4851 (1986).
[43] M. Abramowitz and I. A. Stegun, *Handbook of Mathematical Functions* (Dover, New York, 1965).